JCB Article

Contraction and polymerization cooperate to assemble and close actomyosin rings around *Xenopus* oocyte wounds

Craig A. Mandato[1] and William M. Bement[1,2]

[1]Department of Zoology and [2]Program in Cellular and Molecular Biology, University of Wisconsin, Madison, WI 53706

Xenopus oocytes assemble an array of F-actin and myosin 2 around plasma membrane wounds. We analyzed this process in living oocytes using confocal time-lapse (four-dimensional) microscopy. Closure of wounds requires assembly and contraction of a classic "contractile ring" composed of F-actin and myosin 2. However, this ring works in concert with a 5–10-μm wide "zone" of localized actin and myosin 2 assembly. The zone forms before the ring and can be uncoupled from the ring by inhibition of cortical flow and contractility. However, contractility and the contractile ring are required for the stability and forward movement of the zone, as revealed by changes in zone dynamics after disruption of contractility and flow, or experimentally induced breakage of the contractile ring. We conclude that wound-induced contractile arrays are provided with their characteristic flexibility, speed, and strength by the combined input of two distinct components: a highly dynamic zone in which myosin 2 and actin preferentially assemble, and a stable contractile actomyosin ring.

Introduction

Localized assembly of dynamic contractile structures is essential for several fundamental cellular processes. During cell locomotion in *Dictyostelium*, for example, F-actin and myosin 2 form a dynamic array at the trailing edge of the cell that provides contractile force necessary for detachment of the cell rear from the substrate (e.g., Jay et al., 1995; Moores et al., 1996). Similarly, during cytokinesis, F-actin and myosin 2 are recruited into a contractile ring around the cell equator that pinches the cell in half (for review see Rappaport, 1996). Likewise, a circumferential ring of F-actin and myosin 2 rapidly assembles around wounds made in the plasma membrane of amphibian oocytes and eggs (e.g., Merriam and Christensen, 1983).

While each of these structures plays a different role and forms in response to different stimuli, they share in common the properties of flexibility and transience. That is, actomyosin rapidly accumulates at the rear of cells in response to polarizing stimuli and reorganizes when the cell stops moving (e.g., Moores et al., 1996; Verkhovsky et al., 1999). In addition, the cytokinetic apparatus can be repositioned by experimental displacement of the spindle (Rappaport, 1996), whereas rings of F-actin and myosin 2 assemble in amphibian oocytes wherever the cell is wounded and disassemble after the completion of healing (Bement et al., 1999).

How does the cell assemble structures that are both sufficiently robust to drive contraction and sufficiently dynamic to respond to changing stimuli? Because the cortex of most cells is comprised of an interconnected network of F-actin and myosin 2, localized contractile structures can in principle be generated as the result of any signal that generates local contraction. Specifically, an initial, localized increase in actomyosin-based contraction is expected to be amplified by the recruitment of actomyosin from adjacent regions due to cortical flow. Cortical flow is the translocation of cortical F-actin, myosin 2, and cell surface proteins parallel to the plane of the plasma membrane (Bray and White, 1988). Such flow is driven by contraction itself, with the integrated cortical cytoskeleton pulling more actomyosin to the site of initial contraction which, in turn, results in greater contractility in that region. Consistent with this notion, cortical flow has been observed during cytokinesis (e.g., Cao and Wang, 1990), pseudocleavage in *Caenorhabditis elegans* (Hird and White, 1993), cell locomotion (e.g., DeBiasio et al., 1996), and experimentally induced contraction in *Xenopus* oocytes (e.g., Benink et al., 2000).

However, several observations are inconsistent with contraction-driven cortical flow being the only mechanism for

The online version of this article contains supplemental material.

Address correspondence to Craig A. Mandato, Department of Zoology, University of Wisconsin, 1117 West Johnson St., Madison, WI 53706. Tel.: (608) 262-5683. Fax: (608) 262-9083. E-mail: camandato@facstaff.wisc.edu

Key words: wound healing; cytokinesis; actin polymerization; dorsal closure; myosin polymerization

The Journal of Cell Biology, Volume 154, Number 4, August 20, 2001 785–797
http://www.jcb.org/cgi/doi/10.1083/jcb.200103105

Supplemental material can be found at:
http://doi.org/10.1083/jcb.200103105

Table I. **Movement rates for actomyosin structures in laser-wounded oocytes**

Movement	Rate[a]	Range	Events measured	Individual measurements	Independent experiments
	μm/min	*μm/min*			
Wound edge	2.5 ± 1.1	0.2–5.8	40	312	11
Comet	11.3 ± 4.7	5.6–19.4	50	356	12
Halo widening	1.5 ± 0.3	1.0–2.1	60	296	10
Cortical flow					
Single particle tracking					
G-actin	3.7 ± 1.1	2.0–4.4	33	209	13
Phalloidin	3.4 ± 0.6	2.8–4.2	23	178	8
Myosin 2	0.7 ± 0.4	0.3–1.9	19	152	6
Kymographs					
G-actin	4.8 ± 1.6	2.5–6.8	50	276	10
Phalloidin	4.1 ± 1.2	2.8–5.1	36	178	9
Myosin 2	0.7 ± 0.9	0.3–2.2	23	152	11

[a]Rates are expressed as mean ± SD.

recruitment of F-actin or myosin 2 to nascent contractile structures. For example, myosin 2 lacking motor activity localizes in the prospective cleavage furrow in *Dictyostelium* (Yumura and Uyeda, 1997; Zang and Spudich, 1998). In addition, in both budding yeast and fission yeast, the initial localization of myosin 2 to the incipient contractile ring is not strictly dependent on F-actin and/or interaction of the myosin 2 with F-actin (e.g., Bi et al., 1998; Lippincott and Li, 1998; Naqvi et al., 1999; Motegi et al., 2000). Further, myosin 2 is found at oocyte wound borders even after disruption of F-actin (Bement et al., 1999).

The *Xenopus* oocyte system is particularly useful for experimental analyses of localized actomyosin recruitment, in that wounds can be produced on demand and in an orientation which facilitates imaging. Here we have analyzed assembly of actomyosin rings in living *Xenopus* oocytes using a combination of laser wounding, time-lapse confocal (four-dimensional [4D]*) microscopy, and experimental manipulation of the actomyosin cytoskeleton. The results reveal that cortical flow and contraction work in concert with de novo assembly of F-actin and myosin 2 to establish and close wound–induced actomyosin arrays.

Results

Four different fluorescent probes for the actomyosin cytoskeleton were used: Alexa 488 (AX)-phalloidin and Texas red (TR)-phalloidin, Oregon green (OG) actin, and tetramethylrhodamine (TMR)-smooth muscle myosin 2. Fluorescent phalloidin has been used to label stable F-actin in cultured cells (Cao and Wang, 1990), sea urchin eggs (Terasaki, 1996), and *Xenopus* oocytes (Benink et al., 2000). Fluorescent actin yields higher background than fluorescent phalloidin, but labels both stable and dynamic F-actin (e.g., Cao and Wang, 1990; Taunton et al., 2000). TMR–myosin 2 serves as a marker for nonmuscle myosin 2A in cultured mammalian cells (Kolega, 1998) and *Xenopus* oocytes (see below). To ensure that the injection, wounding, and imaging regime used for this study did not grossly perturb healing, results obtained by laser wounding and 4D analysis of living oocytes were compared with results obtained by stab wounding and immunofluorescence of fixed oocytes (Bement et al., 1999). These comparisons revealed no differences in any other feature of the healing monitored (data not shown). We also assessed the contribution of calcium-dependent membrane fusion at wound sites to wounds made in the oocyte system. Wounds made in calcium-free medium failed to reseal and injected fluorophores leaked out, indicating that wound-induced actomyosin arrays close on cytoplasm protected by a membrane assembled via calcium-dependent membrane fusion (unpublished data, but see McNeil and Terasaki [2001] and references therein).

Wound-induced actomyosin rings are contractile

If wound closure is based on contraction, two simple predictions follow. First, square wounds should round up as tension is exerted around the wound. Second, elongate wounds should shorten fastest along their long axes. 4D analysis of wound closure confirmed both of these predictions: square wounds produced by the imaging laser rounded up before closure (Fig. 1 A, and Video 1), and oval wounds produced by two rapid, adjacent pulses from the nitrogen dye pump laser closed most rapidly along their long axes until the wound became circular (Fig. 1 B), regardless of the probe used for imaging (Fig. 1 C).

As an alternative means of testing whether circumferential rings of actin are contractile, the distribution of tension in the wound area was assessed by an approach similar to that used for analysis of dorsal closure in *Drosophila* embryos (Kiehart et al., 2000). After injection with OG-actin, oocytes were wounded, allowed to assemble a ring of F-actin, and then rewounded via an imaging laser Z-scan. When rewounded outside the closing ring, the resulting second wounds were narrow ovals, and the original ring continued to close rapidly (Fig. 1 D). However, when the Z-scan was used to generate wounds on the interior of and overlapping with the ring itself, the ring sprang open laterally at the site of damage to the ring, an arc of F-actin formed exterior to the original ring and closure was briefly slowed (Fig. 1 D). Z-line rewounds which contacted the ring were typically 2–2.5 times wider than those which did not contact the ring (Fig. 1 D, and data not shown), as expected if the ring is un-

*Abbreviations used in this paper: AX, Alexa 488; 4D, four-dimensional; NEM, N-ethylmaleimide; OG, Oregon green; TMR, tetramethylrhodamine; TR, Texas red; WGA, wheat germ agglutinin.

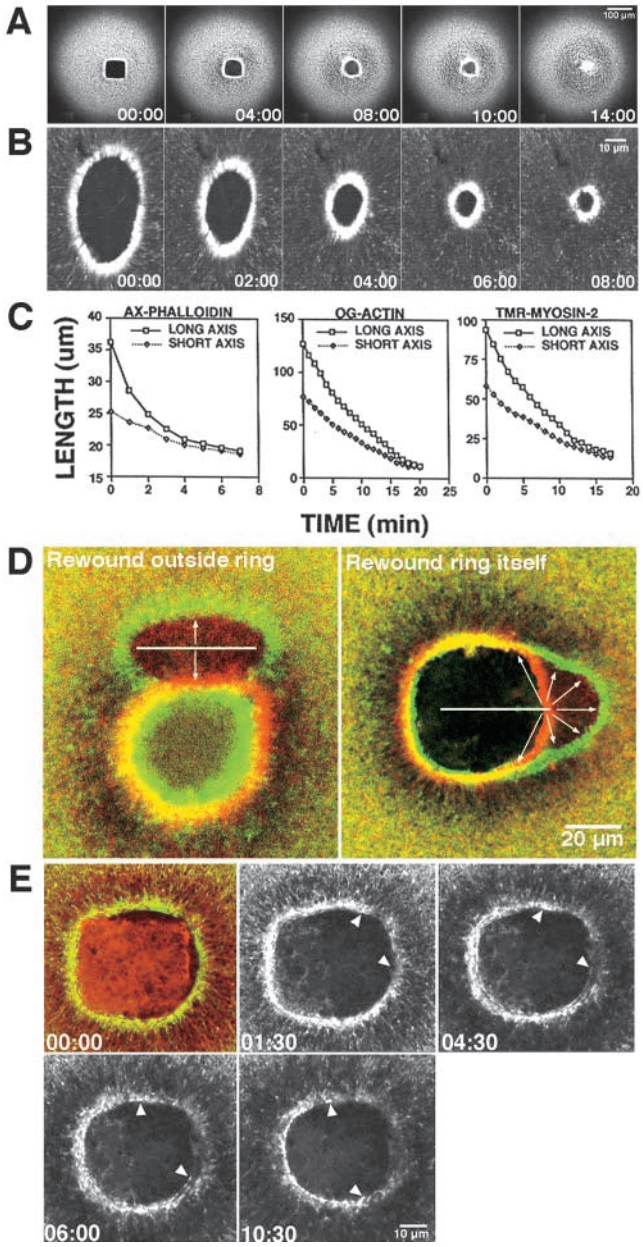

Figure 1. **Wound-induced actomyosin arrays are contractile.** All times are in min:sec. (A) Images from a 4D video of oocyte injected with TR-phalloidin and wounded with imaging laser to produce square wound. Wound rounds up during closure. See Video 1. (B) Images from 4D video of oocyte injected with AX-phalloidin and wounded twice with nitrogen pump laser to generate oval wound. Long axis of wound closes faster than short axis until both are same length. (C) Quantification of oval wound closure. Regardless of probe used, long axes shrink faster than short axes. (D) Fluorescent, color-coded images obtained from 4D videos of oocytes wounded after injection with OG-actin and rewounded either outside the actin ring (left), or on (right) the actin ring. The last image of the 4D video before rewounding is shown in red; the first image taken after rewounding is shown in green. The linear wound made outside the closing ring with a laser Z-scan (white line) is limited in its lateral spread (arrows), whereas the wound made to the ring itself results in the springing open of the ring and extensive lateral spreading (arrows). (E) Fluorescence images from a 4D video of an oocyte injected with AX-phalloidin and TR and then subjected to a "cauterizing" wound (see text). The 00:00 time point is shown in green and red to reveal both the F-actin (green) and the presence of the cauterized region (red square on inside of wound). Subsequent time points show only the phalloidin signal. Closing actin ring breaks on right side of cauterized square and free edges (arrowheads) recoil away from break. See Video 2. The supplemental videos are available at http://www.jcb.org/content/vol154/issue4.

der circumferential tension. Importantly, springing open of the severed ring was limited in recoil to ~15 μm on either side of the Z-scan, implying that the ring is anchored at many points along the wound border.

The above experiments were limited by the fact that after rewounding, 1 min elapsed before imaging resumed (the time required to reconfigure the microscope from a Z-scan to en face imaging). Thus, we were unable to follow the opening of the ring immediately after damage. Further, because wounding itself generates a response, it is impossible to determine to what extent the observed effects of the rewound resulted from previously existing tension versus a response to the rewound. Therefore, we developed a complementary strategy in which wounds were "cauterized" by extending the duration of the laser scan used to create wounds. This produced roughly square regions of burnt cytoplasm within the wound that acted as barriers (Fig. 1 E). Upon contact with the cauterized squares, the ring edges usually either ceased advancement, moved up and over the square, or dove below the square. However, the rings occasionally stretched and broke after contacting the burnt cytoplasm (Fig. 1 E, and Video 2). In such cases, the broken edges of the rings recoiled laterally around the wound toward the unbroken portion, exactly as expected if the ring itself were under circumferential tension. Again, the recoil of the broken edges was limited to ~10–20 μm, and the rest of the ring, after a brief (30–60 s) pause, continued to close, implying that the ring is tightly anchored at many points along its circumference.

Cortical flow creates a vortex of recruitment of stable F-actin to wounds

We next sought to characterize patterns of movement of stable (i.e., previously assembled) F-actin during the wound healing process, since cortical flow is expected to act on stable F-actin. To this end, oocytes were injected with AX-phalloidin, wounded, and imaged. Particle tracking and kymograph analysis of 4D videos showed that stable F-actin flowed toward wounds from cortical regions around the wound edge at ~3 μm/min (Table I), and accumulated in a region of high F-actin density bordering the wound (Fig. 2 A, and Video 3). The flow resulted in the formation of a characteristic dark halo of F-actin depletion around the wound that moved away from the wound over time at a mean rate of 1.5 μm/min (Table I). Flow and halo spreading were independent of the forward movement of the wound edge (data not shown).

High magnification, 4D videos revealed several surprising features of the flow process (Fig. 2, B–E, and Video 4). First, F-actin moved toward the wound in cables oriented perpendicular to the wound border, and then fused with a circumferential array composed of one or two long F-actin cables oriented parallel to the wound border (Fig. 2, B and C, and Video 4). The circumferential cables represent the contractile

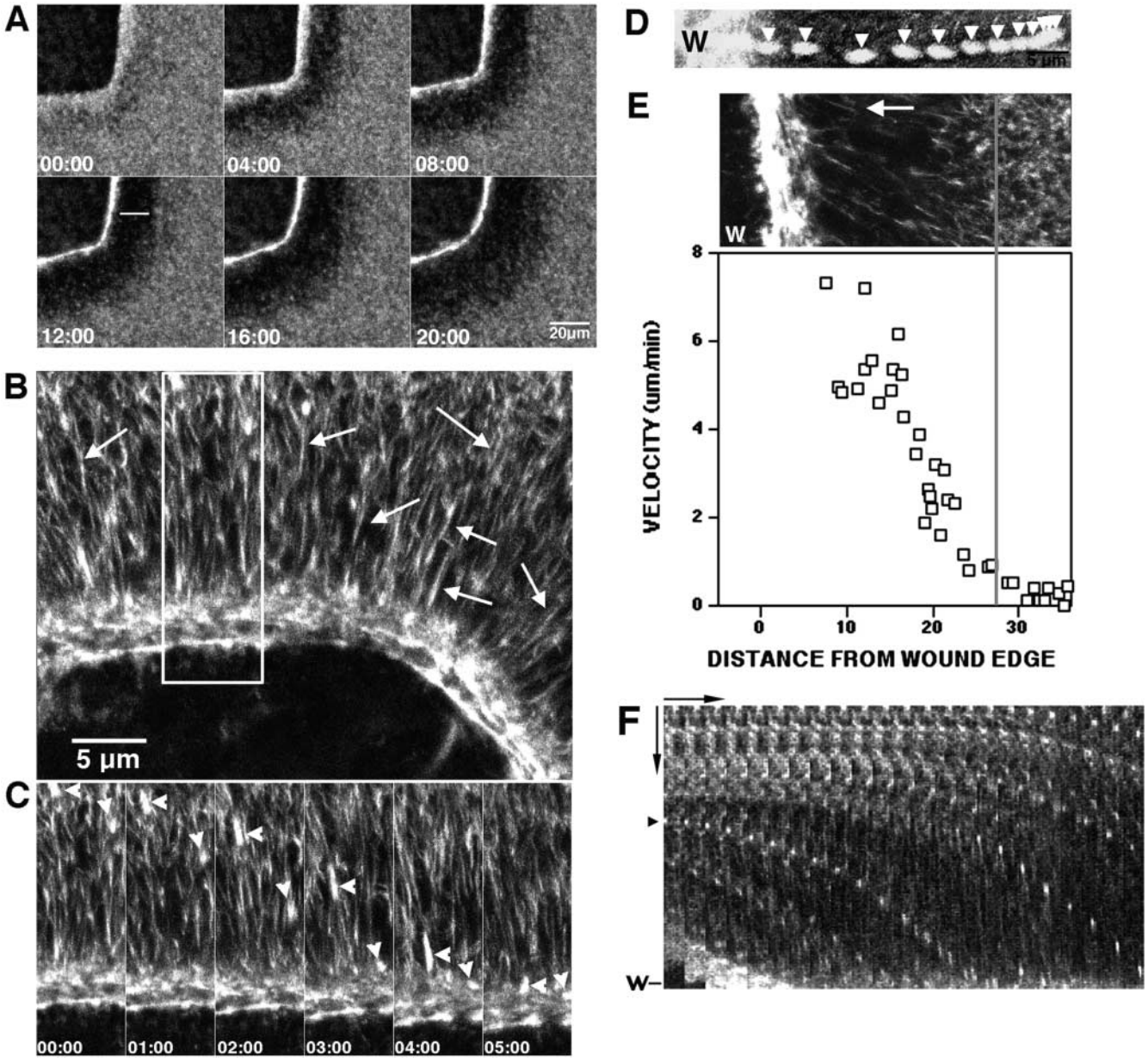

Figure 2. **A vortex of cortical flow at the wound border.** (A) Images from 4D video of wound closure in oocyte injected with AX-phalloidin. Stable F-actin flows from surrounding cortex to wound edge, creating dark halo of F-actin depletion (white line) that spreads from the original wound edge. See Video 3. (B) Image from a 4D video of wound closure in an oocyte injected with AX-phalloidin. Stable F-actin around wound edge is in cables oriented parallel to wound border, whereas peripheral F-actin forms cables oriented perpendicular to wound border (arrows). (C) Images representing boxed area in B. The perpendicular actin cables (arrowheads) flow toward wound edge. See Video 4. (D) Projection of 14, 1 min frames from a 4D video of F-actin particle moving to wound border (W). Over time, F-actin (arrowhead) moves increasing distances toward the wound. (E) Correlative plot of F-actin cable velocity versus distance from the wound. The fluorescence micrograph is taken from the 4D video used to generate the instantaneous velocity measurements shown in the graph; X-axis of the graph corresponds to the area from the micrograph where the measurements were made. Instantaneous velocity measurements show that F-actin more than ~28 μm away from the wound moves slowly; in regions close to wound, rate of movement increases sharply until plateau near wound edge. The threshold distance is correlated with the transitional area between low and high cortical F-actin (gray line). (F) Kymograph of AX-phalloidin–labeled actin motility at the wound edge. Horizontal arrow is 90 s; vertical arrow is 10 μm. Acceleration of F-actin as it approaches wound (W) is revealed by progressively greater distances moved over time by individual actin spots (arrowhead). The supplemental videos are available at http://www.jcb.org/content/vol154/issue4.

ring, in that they snap on contact with barriers (see above) and colocalize with myosin 2 (see below). Second, tracking of single cables followed over multiple time points (Fig. 2 D), instantaneous velocity measurements of multiple cables (Fig. 2 E), and kymograph analysis (Fig. 2 F), revealed that flowing F-actin displayed a sigmoidal pattern of velocity changes as it approached the wound edge: cables moved slowly or not at all beyond a threshold distance from the edge, accelerated as they approached the edge, and then reached a peak speed near the edge (Fig. 2, D–F). Third, the

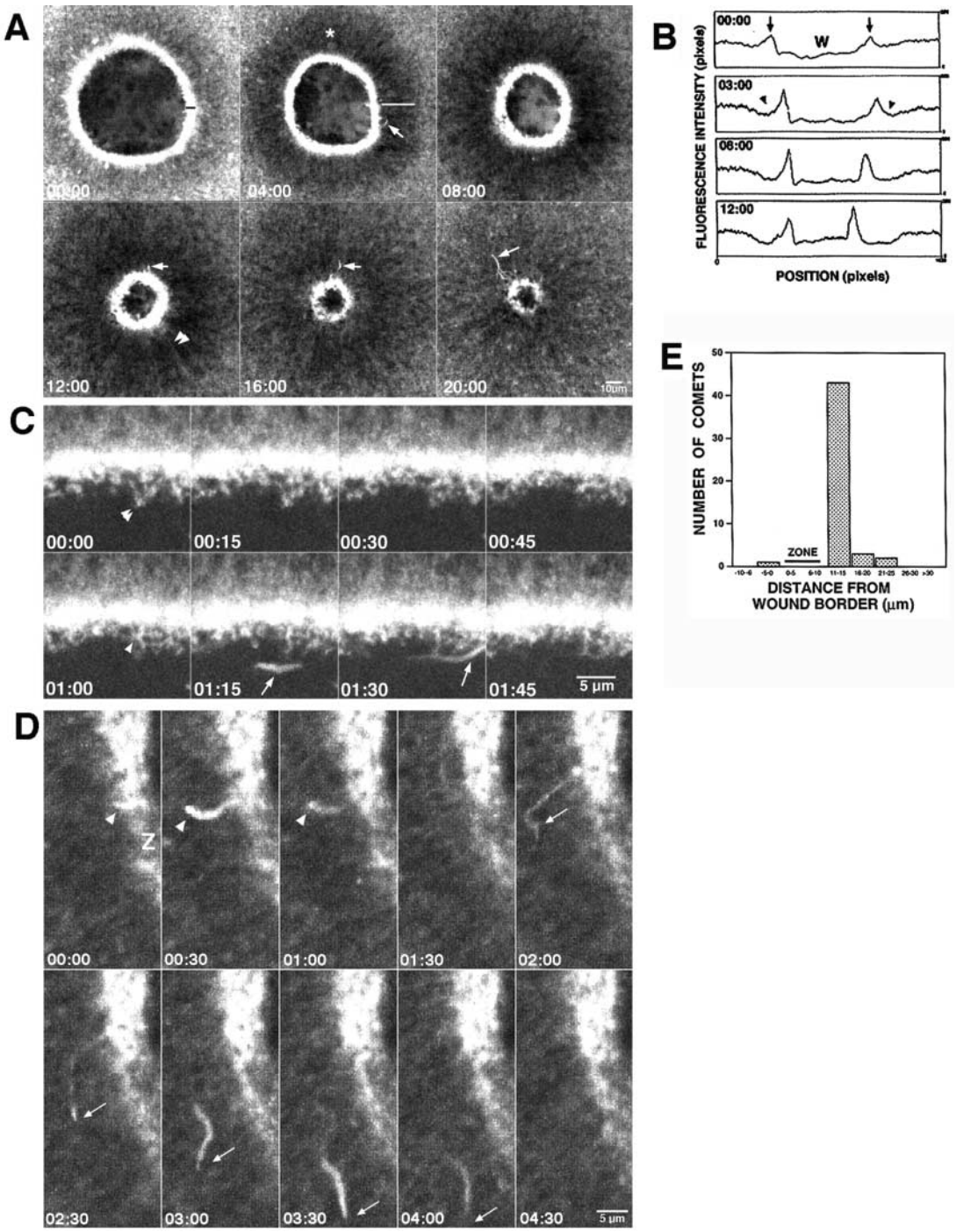

Figure 3. **A zone of highly dynamic actin forms around wounds.** (A) Images from a 4D video of oocyte injected with OG-actin and wounded. Actin is concentrated in an ~6-μm wide zone around wound (black line) that broadens over time and is the site of actin comet formation (arrows). Zone is flanked by dark halo of F-actin depletion (white line). Radial actin cables run perpendicular to the wound border (arrowheads) and disappear into zone of intense actin accumulation. See Video 5. (B) Fluorescence intensity scans from 4D video images of wounds made in an OG-actin–injected oocyte (note that imaging was started much sooner than in Fig. 3 A). At the start (00:00), peaks of F-actin signal (arrows) are evident next to wound (W) even though little depletion of signal is seen in flanking regions. However, at later time points, increasingly prominent signal "troughs" (arrowheads) flanking the peaks are evident. (C) Images from 4D video of oocyte injected with OG-actin and wounded. Wound edge is shown. Actin-rich "fingers" (arrowhead) extend from zone of high actin signal and vanish within 1 min. Fingers often appear to contact each other (double arrowheads). An F-actin comet (arrow) swims lazily through wound area. See Video 6. (D) Images from 4D video showing comets form in or near zone of high actin density (Z). Comets typically taper at one (arrowhead) or both (arrows) ends. See Video 7. (E) Histogram showing relationship between comet position and the zone of high actin intensity. Individual comets that moved more than two frames were followed in 10 experiments. The supplemental videos are available at http://www.jcb.org/content/vol154/issue4.

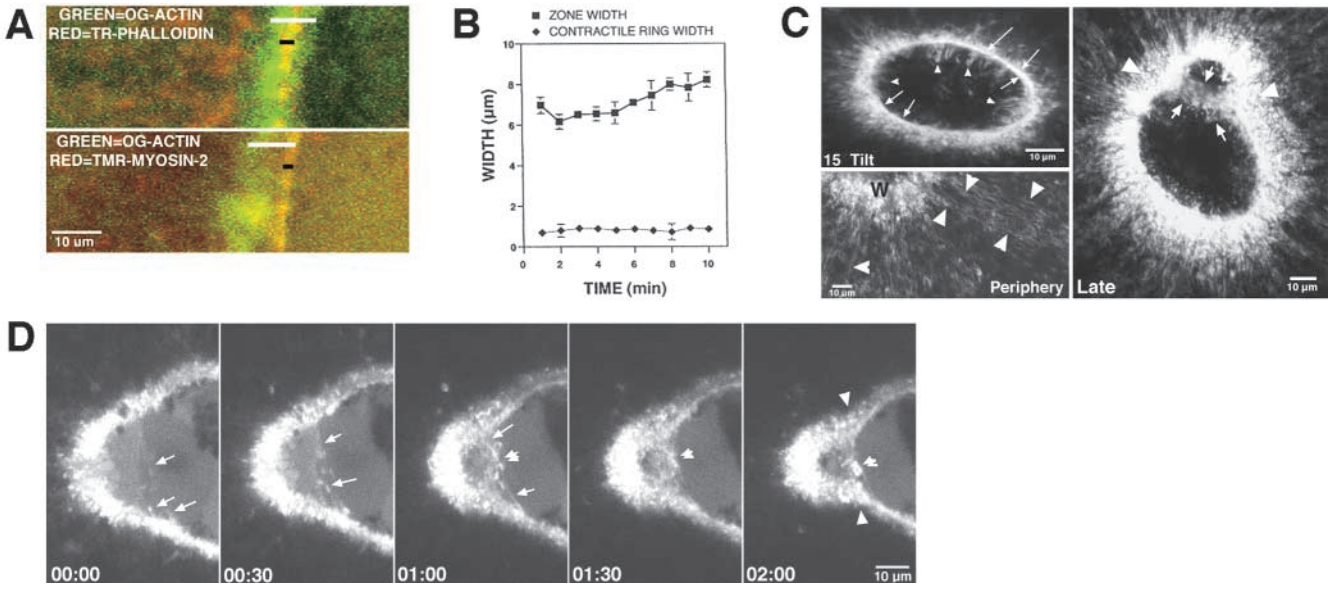

Figure 4. **The contractile ring is contained within the zone of actin polymerization.** (A) Double label images from 4D videos made of oocytes injected with OG-actin and either TR-phalloidin (top) or TMR–myosin 2 (bottom). The TR-phalloidin and TMR–myosin 2 (red) act as markers for the contractile array of F-actin, which forms a tight band (black bar) within the broader zone of polymerization revealed by the green OG-actin (white bar). (B) Quantification of zone and contractile ring width from 4D videos made of oocytes injected with both OG-actin and TR-phalloidin. Zone is ~5 times broader than the contractile ring and increases in width over time. Results are mean ± SEM from three independent experiments. (C) Fluorescence images of F-actin distribution in wounded oocytes stained with phalloidin after fixation. A 15° tilt of an image of a 4-μm stack reveals cables of F-actin parallel to the wound border (arrows) as well as fingers of F-actin extending into the wound (arrowheads). An en face view of the periphery of the wound (periphery) made from a 1.2-μm stack reveals cables of F-actin running perpendicular to the wound border (arrowheads). An en face view made from an 8-μm stack of wound fixed late in healing process (late) reveals F-actin fingers contacting each other across wound (arrows) and apparently pulling the sides of wound together as revealed by indentations in the F-actin array around the wound (arrowheads). (D) Images from a 4D video of an oocyte wound in the late stages of healing. Fingers of F-actin (arrows) contact each other across the wound, shorten over time, and pull edges of wound together, causing indentations actin array around wound (arrow heads). In region of finger contact in middle of the wound, F-actin staining becomes progressively brighter (double arrowheads). See Video 8. The supplemental video is available at http://www.jcb.org/content/vol154/issue4.

threshold distance was correlated with the edge of the halo of F-actin depletion around the zone (Fig. 2 E), indicating that the depletion resulting from flow promotes further flow.

De novo polymerization of actin around wound borders

To characterize contributions of de novo polymerization to contractile ring assembly, oocytes were injected with OG-actin, wounded, and analyzed by 4D microscopy. After assembling a ring of actin around wounds, OG-injected, wounded oocytes displayed perpendicular F-actin cables which flowed toward wound borders, as well as a dark halo of actin depletion around the wound, consistent with results obtained from AX-phalloidin–injected oocytes (Fig. 3 A, and Video 5). Fluorescence intensity measurements revealed the dark halo of the F-actin signal around wounds as a trough between the "background" signal at regions distal to the wounds and the peak signal bordering the wound (Fig. 3 B). Comparison of intensity scans taken at increasing times after wounding demonstrated that at early time points (before those shown in Fig. 3 A), the trough was minimal or absent, but it became quite pronounced at later points, showing that accumulation of F-actin at wound borders precedes the onset of cortical flow.

High magnification videos of OG-actin–injected oocytes indicated that wounding induced de novo polymerization of actin, and that this polymerization was particularly concentrated in the zone of high actin density immediately flanking wound borders. This zone was characterized by the formation of actin-rich "fingers" that extended into the wound region (Fig. 3 C, and Video 6). The fingers were ~0.5–3 μm in length and formed and disappeared within 1 min. The actin-rich zone was also the site of formation of actin comets of ~2–10 μm that appeared, moved through the cortex, and disappeared on a time scale of 30 s to 2 min (Fig. 3, A and D, and Video 7). Such comets have been characterized in both *Xenopus* egg extracts (e.g., Ma et al., 1998) and intact *Xenopus* eggs (Taunton et al., 2000), and are known to reflect de novo actin assembly. Comets moved at an average rate of 11 μm/min (Table I) and were most frequently seen outside the F-actin–rich zone around the wound borders, although they were occasionally observed in the interior of the wound (e.g., Fig. 3 C, and Video 6). Quantitative analysis of the position at which comets first formed revealed that they formed most frequently within 10 μm of the wound edge, corresponding to the zone of high actin density (Fig. 3 E).

To characterize the spatial relationship between stable and dynamic F-actin, two additional experiments were conducted. First, oocytes were injected with TR-phalloidin as a marker for stable F-actin and then OG-actin as a probe for dynamic F-actin. After wounding, the stable F-actin was localized as a narrow ring around wounds within a broader ring composed of dynamic F-actin (Fig. 4 A). Likewise, double labeling with OG-actin and TMR–myosin 2 revealed that the

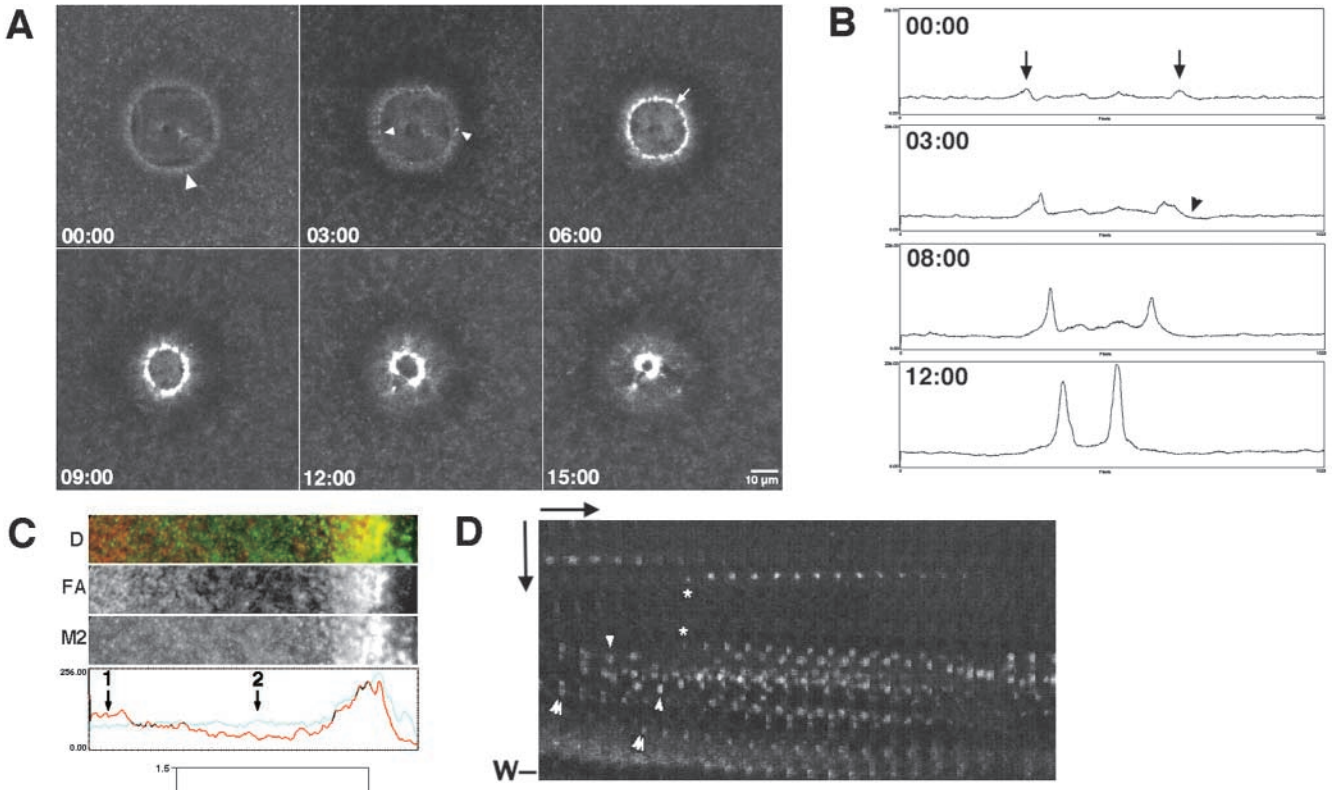

Figure 5. **Myosin 2 accumulates around wounds with little obvious flow.** Time shown is in min:sec. (A) Images from 4D video of oocyte injected with TMR–myosin 2 and wounded. Bright foci of myosin 2 (arrowheads) accumulate around wound border and eventually fuse into tight, continuous ring (arrow). See Video 9. (B) Fluorescence intensity scans from 4D video images of wounds made in TMR-myosin 2–injected oocyte. At start of imaging (00:00), peaks of myosin 2 signal (arrows) are evident flanking wound (W) even though no depletion of signal is seen in the flanking regions. Even at later time points, the signal trough (arrowhead) flanking signal peaks are quite limited relative to those seen with actin probes (compare to Fig. 3 B above). (C) Confocal, double-labeled image (D) of a wound edge stained for F-actin (FA) and myosin 2 (M2) with a corresponding signal intensity plot, where the red line is F-actin signal and the blue line is myosin 2 signal. Quantification of signal from region 1 (beyond the dark halo of depletion) versus region 2 (in the dark halo) shows that the degree of F-actin depletion in the dark halo is significantly greater than that of myosin 2 (results are mean ± SEM; asterisk indicates $P < 0.05$; $n = 20$ wounds from 3 experiments). (D) Kymograph of TMR-myosin motility at wound edge. Horizontal arrow is 45 s; vertical arrow is 10 μm. Some myosin 2 foci move toward the wound at the same rate as the edge moves forward (double arrowheads); some move backward (arrowheads) and some new foci appear during the course of imaging (asterisks). Few foci show acceleration toward the wound edge seen for F-actin (compare to Fig. 2 F). (E) Vector plot diagram of myosin 2 foci movement from Video 10. Each point is separated by 15 s; some foci move steadily toward wound (W), some move intermittently, and some move parallel to wound edge. Asterisks represent areas where foci appeared during the course of imaging. See Video 10. The supplemental videos are available at http://www.jcb.org/content/vol154/issue4.

myosin 2 was focused as a narrow ring within a broader ring of dynamic F-actin (Fig. 4 A). While the width of the zone of dynamic F-actin increased over time, the width of the contractile actomyosin ring remained constant (Fig. 4 B).

Second, total F-actin distribution was analyzed in wounded, fixed oocytes stained with TR-phalloidin. Three-dimensional reconstructions of such oocytes revealed the features observed above, including perpendicular F-actin cables, parallel F-actin cables within a broader ring of disorganized F-actin, and F-actin fingers extending into the interior of the wound (Fig. 4 C). Thus, the novel dynamic features of the healing process observed above result from neither the probes used for injection nor the injection process itself. These experiments had an additional important outcome: during analysis of oocytes fixed late in the process of healing, it was found that the fingers of F-actin stretched across the wound, contacting each other and apparently pulling the edges of the wound together (Fig. 4 C). These findings were corroborated by 4D analysis: as healing neared completion, fingers extended across the wounds and shortened, pulling the wound shut (Fig. 4 D, and Video 8).

Myosin 2 accumulates around wounds with only limited recruitment from the cortex

To monitor recruitment of myosin 2 to wound borders in vivo, oocytes were injected with TMR–myosin 2, and then

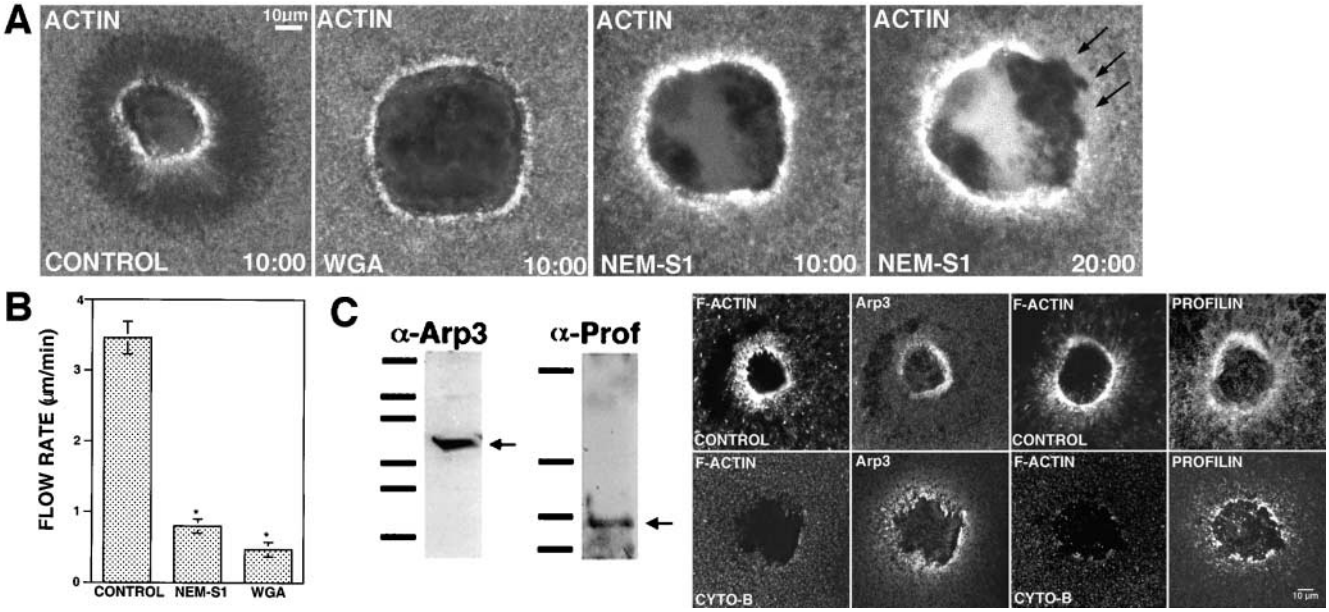

Figure 6. **Uncoupling actin assembly from cortical contraction and flow.** (A) Images from 4D videos made of oocytes injected with OG-actin and then wounded. After 10:00 min, control wound (control) has rounded up and begun closure and shows typical F-actin distribution, including flow-dependent formation of a dark halo around the wound. In contrast, when flow is blocked by treatment with 100 ug/ml WGA or injection of 4 mg/ml NEM-S1, rounding and closure are perturbed and the dark halo fails to appear. Nevertheless, a zone of actin polymerization still forms around wounds. However, at later time points, the zone becomes destabilized and disappears from around wound (NEM-S1, 20:00). (B) Quantification of cortical flow inhibition by 4 mg/ml NEM-S1 and 100 μg/ml WGA. Cortical flow rates were calculated from 4D videos made from oocytes subjected to the indicated treatments. Results are mean ± SEM of three independent experiments; asterisk indicates $P < 0.001$. (C) Immunoblot (top) analysis of *Xenopus* egg extracts shows that antibodies to Arp3 (α-Arp3) and profilin (α-Prof) recognize proteins from *Xenopus* egg extracts of 50 and 15 kD, respectively (arrows). Bars indicate molecular weight markers of 211, 128, 84, 42, 32, and 17 kD (Arp3 blot) and 38, 29, 18, and 9 kD (profilin blot). In both absence (control) and presence (cyto-B) of 40 μM cytochalasin, profilin and Arp3 accumulate around wounds.

wounded and analyzed as above. After wounding, TMR–myosin 2 rapidly accumulates around wound borders in bright foci that fuse to form a continuous, circumferential ring that closes with time (Fig. 5 A, and Video 9). Analysis of myosin 2 dynamics revealed two principle differences relative to actin: myosin 2 flow was much less obvious than F-actin flow, and myosin 2 was present in regions bordering the wound as punctae rather than continuous cables (Fig. 5 A, and Video 9). The lesser degree of flow was also apparent as reduced myosin 2 depletion in wound-flanking regions detected by fluorescence intensity measurements of both living (Fig. 5 B) and fixed samples (Fig. 5 C).

To investigate the basis of this difference, myosin 2 dynamics were analyzed by 4D microscopy in greater detail at high magnifications and shorter sampling intervals, followed by both kymograph (Fig. 5 D) and single particle tracking (Fig. 5 E) analysis. This revealed three features of myosin 2 dynamics that could account for the apparent difference in cortical flow. First, although some myosin 2 punctae moved toward the wound, the patterns of movement were distinctly different than those of F-actin. That is, flow of myosin 2 to wound borders was intermittent, with individual punctae exhibiting frequent starts and stops (Fig. 5, D and E, and Video 10). Further, many of the punctae did not move directly toward the wound edge, but instead moved parallel to the wound border or even away from the wound border. Second, some of the myosin 2 moved forward at the same rate as the leading edge of the wound edge, as if being moved via stretching of the cortex (Fig. 5 D). Third, new myosin 2 punctae appeared continuously in the region where flow was occurring, replacing those that moved toward the wound edge (Fig. 5, D and E, and Video 10). In contrast to the flow of F-actin, very few myosin 2 punctae displayed the acceleration observed for F-actin (compare Figs. 5 D and 2 F).

A zone of actin polymerization around wound borders

The foregoing results suggested that both F-actin and myosin 2 can accumulate around wounds by mechanisms independent of contraction-dependent cortical flow. To test this point directly for F-actin, oocytes were subjected to treatments designed to prevent cortical flow and/or contraction. Cortical flow can be prevented by incubation of oocytes in high concentrations of lectins, such as wheat germ agglutinin (WGA), which crosslinks cell surface proteins, thereby immobilizing the cortex (Canman and Bement, 1997). In WGA-treated oocytes, wound-induced cortical flow was inhibited, no dark halo formed, and wounds failed to round up and close (Fig. 6, A and B). Nevertheless, F-actin still accumulated in a zone around wounds in WGA-treated oocytes, although the zone was unstable (Fig. 6 A). As an alternative approach, oocytes were injected with N-ethylmaleimide (NEM)-treated S1, which binds specifically and irreversibly to the myosin binding site of F-actin, and thereby inhibits contractility (Meeusen and Cande, 1979). NEM-S1 inhibited cortical flow, wound rounding up, and wound closure; how-

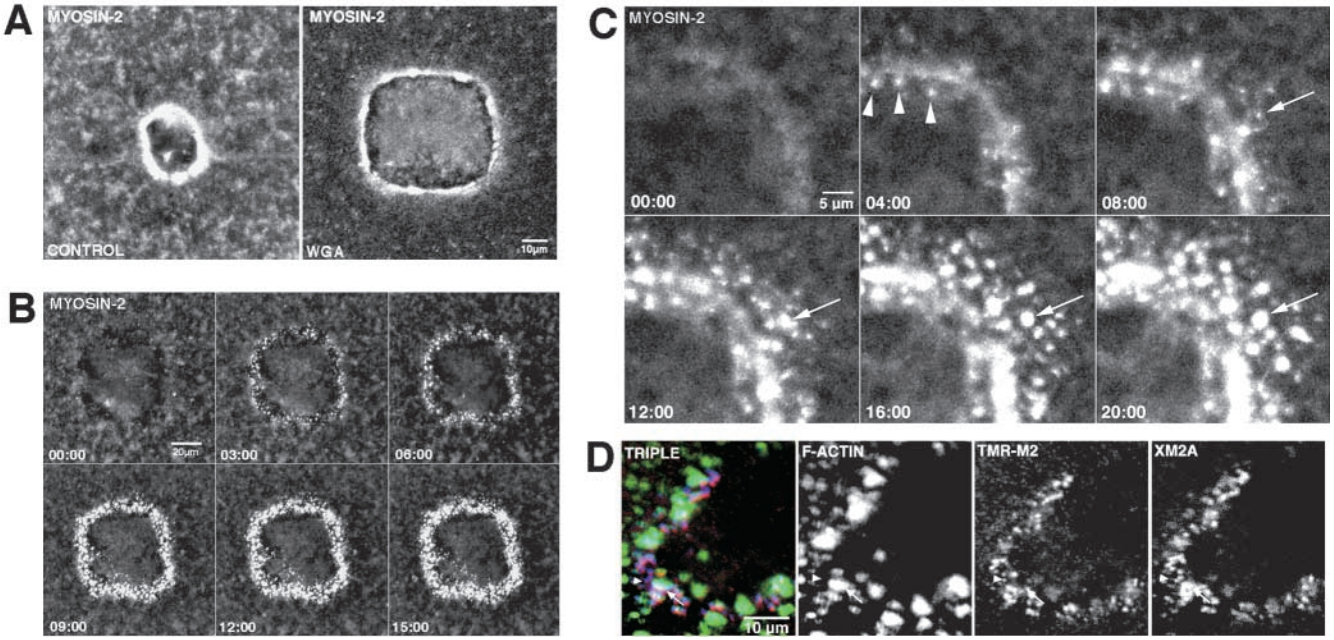

Figure 7. **Uncoupling myosin assembly from cortical contraction and cortical flow.** (A) Images from 4D videos made from oocytes injected with TMR–myosin 2 and wounded. After 10 minutes, the control wound (control) has rounded up, commenced closure, and assembled a smooth, continuous ring of myosin 2. In contrast, the wound from oocyte treated with 100 μg/ml WGA was not rounded up nor closed, yet myosin 2 accumulated around the wound border in an irregular, discontinuous array. (B) Images from oocyte injected with TMR–myosin 2 and then wounded after treatment with 40 μm cytochalasin B. Bright foci of myosin 2 accumulate over time around wound border, but fail to coalesce into a continuous ring. (C) High magnification images from a 4D video of oocyte injected with TMR–myosin 2 and wounded after cytochalasin treatment. At the start of imaging (00:00), myosin 2 is visible as faint band. Bright foci of myosin appear adjacent to this band (arrowheads), and band is eventually surrounded by a ~5–10-μm zone of myosin 2 foci (20:00). Most individual myosin 2 foci (e.g., arrow) grow progressively larger over time in the absence of any apparent transport. See Video 11. (D) Triple-label, confocal fluorescence analysis showing F-actin (green), TMR–myosin 2 (red), and endogenous myosin 2A (blue) in oocytes wounded after pretreatment with cytochalasin. TMR–myosin 2 (TMR-M2) and endogenous myosin 2A (XM2A) are codistributed around the wound. In some cases, they overlap with F-actin which remains after cytochalasin treatment (arrow), but in other cases they do not (arrowhead). The supplemental video is available at http://www.jcb.org/content/vol154/issue4.

ever, as with WGA, actin accumulated around wound borders (Fig. 6, A and B). The actin accumulation was unstable and eventually disappeared from the wound border (Fig. 6 A).

If wounding generates a zone of actin polymerization around the wound which is independent of the contraction- and flow-dependent accumulation of F-actin, proteins upstream of actin polymerization should be concentrated around wounds even when F-actin polymerization is inhibited. To test this point, control oocytes and oocytes pretreated with cytochalasin were wounded, fixed, and then immunostained using antibodies raised against Arp3 and profilin, both of which are upstream participants in F-actin polymerization (e.g., Welch, 1999). Immunoblotting of *Xenopus* egg extracts with anti-Arp3 and antiprofilin showed that the antibodies recognize *Xenopus* proteins of 50 and 15 kD, respectively, which is the expected size of these proteins (Fig. 6 C). Enrichment of both Arp3 and profilin around wound borders was evident in control oocytes as well as oocytes pretreated with cytochalasin (Fig. 6 C), indicating that wounding results in an upstream stimulus for actin polymerization around wounds.

Uncoupling of myosin 2 recruitment from cortical flow and contraction

To test whether myosin 2 recruitment to wound borders requires cortical flow or contractility, oocytes were injected with TMR–myosin 2, treated with WGA to block cortical flow, wounded, and then analyzed by 4D microscopy. As with actin (see above), WGA treatment failed to prevent the accumulation of TMR–myosin 2 to wound borders, although it failed to coalesce into a tight circumferential array (Fig. 7 A). As an alternative means of preventing contraction and cortical flow, TMR-myosin 2–injected oocytes were treated with cytochalasin and then wounded. After wounding, myosin 2 accumulated around the wound border in bright foci which failed to coalesce in a continuous ring (Fig. 7 B). Higher magnification videos revealed that such foci formed and grew progressively larger in the absence of any apparent recruitment from cortical regions (Fig. 7 C, and Video 11).

To assess the distribution of myosin 2 foci with respect to the punctae of F-actin that remain after cytochalasin treatment and to confirm that injected TMR–myosin 2 acts as a faithful marker for endogenous myosin 2A, oocytes were injected with TMR–myosin 2, treated with cytochalasin, wounded, fixed, and then processed for triple labeling. Confocal analysis showed that the TMR–myosin 2 foci were colocalized with endogenous myosin 2A and, further, that these myosin 2 foci could be found in the absence of associated F-actin (Fig. 7 D). Thus, neither F-actin nor flow of cortical myosin 2 are required for accumulation of myosin 2 around the wound, although F-actin and contractility are re-

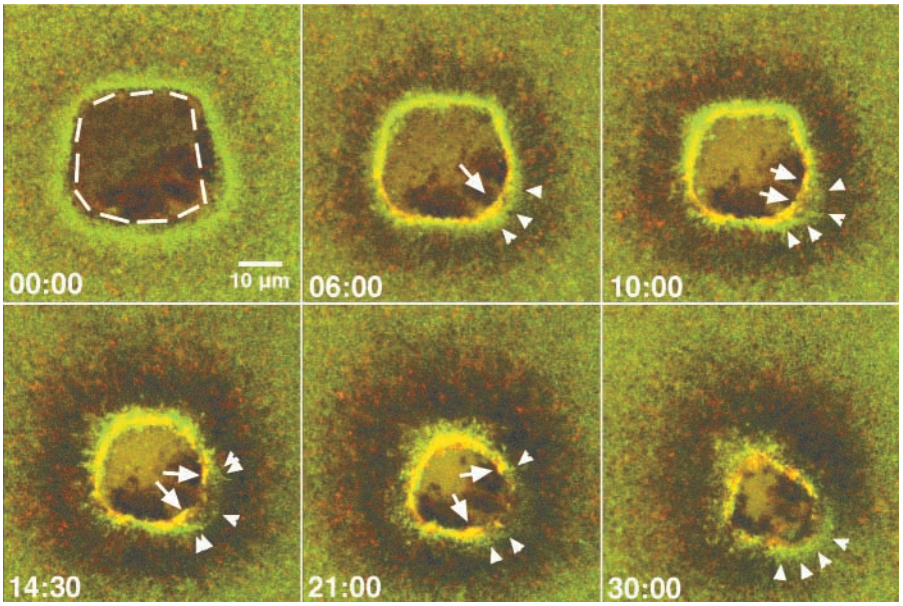

Figure 8. **Breakage of the contractile ring destabilizes the zone of actin polymerization.** Double-label images from 4D video of oocyte injected with OG-actin and TMR–myosin 2 and then subjected to cauterization wounding. See Video 12. Hatched line indicates burnt area of cytoplasm. Initially actin is present around wound as typical zone of polymerization. 6 min after start of imaging cortical flow has commenced, as revealed by development of dark halo around wound. The contractile ring is visible as a tight red-yellow ring within broader green zone of polymerization. The ring encounters edge of cauterized cytoplasm (arrow), stops movement, and begins to stretch. The zone of actin polymerization is broader in this region (arrowheads). By 10 min the contractile ring has broken, two recoiling free edges are visible (arrows) and zone widens and dims locally near break. At later time points (14:30) the edge of the spreading zone (arrowhead) is only barely visible near the original break site, whereas the spreading itself (double arrowheads) is apparently following the retreating free edges of the broken contractile ring (arrows). By 21 min the zone is almost gone near the original break point, but by 30 min, a new zone has assembled (arrowheads). The supplemental video is available at http://www.jcb.org/content/vol154/issue4.

quired for myosin 2 to form a continuous ring around the wound and for the wound to close.

Breakage of the contractile ring causes localized destabilization of the polymerization zone

The fact that actin and myosin 2 accumulated around wound borders when contraction and cortical flow were prevented demonstrated that neither contractility nor the contractile ring are required for formation of the polymerization zone. However, the fact that the zone eventually disappeared in the presence of NEM-S1 and WGA suggested that contractility, the contractile ring, or both help maintain the zone. To test this notion, oocytes were injected with both OG-actin and TMR–myosin 2, and then subjected to wound cauterization. The TMR–myosin 2 allowed identification of the contractile ring within the broader zone of polymerization revealed by OG-actin (Fig. 4 A). Upon contact with the cauterized region, one portion of the contractile ring ceases movement, becomes stretched, and then snaps (Fig. 8 and Video 12). The local stopping and stretching of the contractile ring was accompanied by local stopping and broadening of the polymerization zone (Fig. 8 and Video 12). Upon breakage of the contractile ring, the zone transiently disappeared and then reappeared as an arc extending off of the rest of the actomyosin array around the wound, but distal from the wound edge. Thus, the contractile ring is required for forward movement of the zone and to keep it focussed around the edge of the wound. The supplemental videos are available at http://www.jcb.org/content/vol154/issue4.

Discussion

The first finding of this study is that actomyosin rings induced by wounding of *Xenopus* oocytes are contractile. The mere presence of a shrinking, circumferential ring of F-actin cannot be assumed to indicate a contractile mechanism per se (Fenteany et al., 2000). However, in the oocyte system the wound-induced actomyosin array is indeed contractile, an important finding if this model system is to be considered relevant to other transient, contractile structures. At the same time, it is also apparent that contractility and forward movement are not strictly dependent on having an intact ring, since forward movement continues on sides opposite of the breaks. This observation, and the fact that broken ring edges are limited in their recoil, imply that wound-induced contractile rings are firmly anchored to the plasma membrane at frequent intervals along their length. This is consistent with work in *Drosophila* embryos showing that the actomyosin array required for dorsal closure is contractile, but still advances after damage to one edge (Kiehart et al., 2000).

The second finding is that F-actin cables flowing toward wounds accelerate sharply as they leave regions of high cortical actin density. This implies the existence of a positive feedback loop in which flow-dependent depletion of F-actin promotes further, rapid recruitment of F-actin, which in turn results in additional depletion. This observation provides direct, empirical support for cortical flow–dependent positive feedback in contractile processes, a longstanding, but previously untested notion (e.g., White and Borisy, 1983; Mandato et al., 2000). It also confirms the idea that spatially restricted destabilization of cortical actomyosin may be as important for localized contractile phenomena as contraction itself, an idea recurrent in both the cytokinesis (White and Borisy, 1983; Mandato et al., 2000) and cell locomotion (Taylor and Fechheimer, 1982; DeBiasio et al., 1996) literature.

The third finding, and the most surprising, is the formation of a restricted zone of de novo actin and myosin 2 assembly that works in concert with the classic contractile ring

of continuous cables that run parallel to the wound border. Fluorescence intensity measurements indicate that de novo polymerization provides the initial signal for actomyosin accumulation around wound borders which, in turn, drives recruitment of F-actin via contraction and flow. Whether myosin 2 is also recruited via flow is unclear, since repeated attempts to document continuous flow failed. Instead, myosin 2 foci near the wound moved at the same rate as the wound edge, or in an intermittent manner. Even more surprisingly, myosin 2 foci often moved either perpendicular to or against the direction of flow. Thus, in addition to de novo polymerization, myosin 2 recruitment is mediated by a motility mechanism distinct from that used for F-actin. This result is not predicted by standard models of cortical flow, although we cannot rule out the possibility that myosin 2 that we cannot detect with our methods is also moving by a standard flow-based mechanism.

The results with the flow and contraction inhibitors indicate that, once formed, the polymerization zone is relatively unstable and requires contraction and flow for its maintenance as well as its forward movement. These results were confirmed by cauterization-induced ring breakage: stretching of the ring is accompanied by broadening of the zone, whereas its breakage results in transient disappearance of the zone. While it is easy to understand how contraction of the ring moves the wound edge forward, it is more difficult to understand why the ring is necessary for maintenance of the zone. One possibility is that the ring acts as a moveable scaffold for signaling molecules responsible for de novo assembly of actin and myosin 2.

An additional role for the zone of actomyosin assembly is demonstrated by the finding that late in the process of healing, F-actin fingers on opposing sides of the wound contact each other and pull the wound edges toward each other. The existence and dynamics of the F-actin fingers is remarkable for two reasons. First, in a detailed study of F-actin organization in fixed, cultured cells undergoing cytokinesis, Fishkind and Wang (1993) deduced the existence of ordered arrays of F-actin extending ahead of the cytoplasmic apparatus (see Fishkind and Wang, 1993, Fig. 9). Second, the behavior of the fingers is eerily reminiscent of ventral enclosure in *C. elegans* (Raich et al., 1999) and dorsal closure in *Drosophila* (Jacinto et al., 2000), wherein filapodia extend from and link opposing epithelial cells at the midline of the embryo. Consistent with our findings, Jacinto et al. (2000) found that in *Drosophila* this mechanism is operative primarily in the late stages of dorsal closure, and that the contacting filapodia exert force on the epithelial margin, as judged by its inward bending at points of contact (Jacinto et al., 2000). Obviously, the fingers differ from filapodia found in moving epithelia in that they are contained within a single cell. Nevertheless, their association with a contractile ring further supports the assertion that diverse, contractile ring–dependent events may have conserved evolutionary roots (e.g., Bement et al., 1999; Woolley and Martin, 2000).

Whether a localized zone of actomyosin polymerization is also a component of other contractile structures remains to be seen, but this possibility could account for recent findings from *Dictyostelium* and yeast (see Introduction). The observations in fission yeast are especially striking in that they show discrete myosin 2 foci at the fission site in the absence of F-actin (Motegi et al., 2000). In addition, it was recently found that myosin 2 accumulates ahead of actin in cleavage furrows in *Xenopus* embryos (Noguchi and Mabuchi, 2001), suggesting that its recruitment may be F-actin–independent. Local regulation of myosin 2 and actin assembly during cytokinesis is also consistent with studies suggesting local control of myosin 2 regulatory light chain phosphorylation (e.g., DeBiasio et al., 1996; Matsumura et al., 1998; Poperechnaya et al., 2000) and the dependence of cytokinesis on proteins that regulate actin assembly and disassembly (e.g., Balasubramanian et al., 1994; Gunsalus et al., 1995), respectively.

What cellular and molecular mechanisms underlie the zone of actin and myosin 2 assembly? Three nonexclusive mechanisms are suggested by the literature: (a) Cdc42 is a likely candidate since the zone is the site of comet formation and comet formation is Cdc42-dependent in *Xenopus* egg extracts (e.g., Ma et al., 1998). (b) Likewise, PIP2 regulates F-actin comet formation in cultured cells (Rozelle et al., 2000), suggesting that this lipid might also be involved in actin dynamics in the polymerization zone. (c) Similarly, PKCs may act upstream of one or more of the rho class GTPases, since PKC agonists trigger formation of comets in *Xenopus* eggs (Taunton et al., 2000). Regardless of the upstream players, the polymerization zone is subject to very tight spatial control: neither F-actin nor myosin 2 spread far into the wound or far away from it. At the same time, the zone is resilient, disappearing and reappearing after stretching and breakage of the contractile ring, or rapidly assembling as an arc off of a severed ring.

In summary, the combined input of a contractile ring and a zone of actomyosin polymerization endow wound-induced actomyosin arrays with the strength, speed, and flexibility necessary for efficient assembly and closure. Therefore, it will be of interest to see if polymerization zones are associated with the contractile arrays that drive cytokinesis, morphogenesis, and multicellular wound healing. It will also be important to determine how the cell generates and controls such zones in response to wounding.

Materials and methods

Oocyte acquisition, microinjection, and manipulation

Oocytes were obtained from adult *Xenopus* females, defolliculated, and stored in OR 2 (82.5 mM NaCl, 2.5 KCl, 1 mM $CaCl_2$, 1 mM $MgCl_2$, 1 mM Na_2HPO_4, and 5 mM Hepes, pH 7.4). Fluorescent probes were pressure injected with glass microneedles. Before injection, fluorescent proteins were thawed from −80°C stocks, diluted to the injection concentrations, and centrifuged at 100,000 *g* for 30 min at 4°C. To visualize actin, in vivo oocytes were injected at the equatorial region with either OG-labeled G-actin at a concentration of 3 mg/ml (a gift from Dr. Clare Waterman-Storer, Scripps Research Institute, La Jolla, CA), or TR- or AX-phalloidin (Molecular Probes) at a concentration of 2 U/ml in 5 mM Tris-acetate buffer, pH 6.8. To visualize myosin, in vivo oocytes were injected with TMR-labeled smooth muscle myosin at 4 mg/ml. Smooth muscle myosin was prepared from turkey gizzards and labeled with TMR maleimide (Molecular Probes) at a dye/protein molar ratio of 5:1 and stored by drop freezing in liquid nitrogen. NEM-myosin was prepared as described by Meeusen and Cande (1979).

Laser wounding

Laser wounds were made through a 10 or 25× objective with either a Micropoint pulse nitrogen–pumped dye laser (Laser Science, Inc.) or with a Krypton/Argon Bio-Rad Laboratories imaging laser (American Laser Corporation). Oocytes were placed between a glass slide and a coverslip sepa-

rated by grease and positioned in the laser path. Wounding with the nitrogen laser, which emitted 120 uJ of 337 nm energy in 2-ns pulses (15.9 mW/cm^2 at the cell surface) resulted in small, round wounds. Wounding with the imaging laser using both 488- and 586-nm laser lines at 100% power (3.7 mW/cm^2 at the cell surface) produced square wounds.

4D live Imaging

All 4D imaging was performed using a 100 M microscope (Axiovert; Zeiss) with the Bio-Rad 1024 Lasersharp Confocal software package. For each time interval, 9–12 1,024 × 1,024 images were collected with a Kalman averaging of 2–3. Step sizes were 0.36–1 μm. 4D videos were constructed from the confocal stacks with the Lasersharp software and imported into NIH Object Image v2.06 for analysis and kymograph construction. Further image analysis and processing were performed with Adobe Photoshop® 5.0, Metamorph 4.5 (Universal Imaging Corp.), Quicktime 4.1.2 (Apple Computer, Inc.) or Adobe Premiere® 5.1. Statistical analysis were performed using Microsoft Excel.

Perturbation of healing

To disrupt cortical flow and actomyosin array formation, oocytes injected with fluorescent probes were preincubated for 1 h in 40 μM cytochalasin B or 100 μg/ml WGA (Sigma-Aldrich) or injected with NEM-S1 at a needle concentration of 4 mg/ml immediately before wounding.

Confocal microscopy of fixed oocytes

After wounding, oocytes were fixed overnight in 40 mM Hepes, pH 7.6, 100 mM KCl, 3 mM $MgCl_2$, 150 mM sucrose, 10 mM EGTA, 0.1% Triton X-100 containing 4% paraformaldehyde, 0.1% glutaraldehyde, and 1 μm taxol. Oocytes were washed for 24 h in TBS containing 0.1% NP-40 (TBSN) and stained in TBSN plus 1 U/ml TR-X-phalloidin (Molecular Probes). After a 24 h wash in TBSN, samples were mounted and viewed. Serial optical sections were collected on a Bio Rad Laboratories 1024 laser-scanning confocal microscope. For double or triple labeling of F-actin, injected myosin 2, and endogenous myosin 2, TMR-myosin–injected oocytes were wounded, fixed, and washed as above, and then stained for F-actin and for endogenous myosin 2 using an affinity-purified *Xenopus* myosin 2A antibody (provided by Dr. Bob Adelstein, National Institutes of Health, Bethesda, MD) as described previously (Bement et al., 1999). Profilin and arp3 antibodies (Welch et al., 1997) were a gift from Dr. Matt Welch (University of California, Berkley, CA) and were used for both immunoblotting and immunofluorescence. Immunofluorescence was as above; for immunoblotting, *Xenopus* egg extracts were separated on 4 20% SDS-acrylamide gels, transferred to nitrocellulose, immunoblotted with the α-profilin and α-arp3 antibodies followed by HRP secondary antibodies, and developed using the ECL Western blotting system (Amersham Pharmacia Biotech).

Online supplemental material

All 4D confocal time-lapse videos were created using Bio Rad Laboratories LaserSharp software and produced in Quicktime 4.1.2 format. Videos are available at http://www.jcb.org/content/vol154/issue4.

We are grateful to Bob Adelstein (National Institutes of Health, Bethesda, MD), Mary Halloran (University of Wisconsin-Madison), Jim Pawley (University of Wisconsin-Madison), John Peloquin (University of Wisconsin-Madison), Clare Waterman-Storer (Scripps Research Institute, La Jolla, CA), and Matt Welch (University of California, Berkeley, CA) for providing reagents, equipment, and advice. We would also like to thank the members of our laboratory for continued support, input, and suggestions, and an anonymous reviewer for two very useful suggestions.

This work was supported by the National Institutes of Health (GM52932-04A1); C.A. Mandato is supported by a Guyer Post-Doctoral Fellowship. The National Science Foundation supported acquisition of the confocal microscope used in this study (NSF9724515 to J. Pawley) and early phases of this project (MCB 9630860).

Submitted: 22 March 2001
Accepted: 10 July 2001

References

Balasubramanian, M.K., B.R. Hirani, J.D. Burke, and K.L. Gould. 1994. The *Schizosaccharomyces pombe* cdc3+ gene encodes a profilin essential for cytokinesis. *J. Cell Biol.* 125:1289–1301.

Bement, W.M., C.A. Mandato, and M.N. Kirsch. 1999. Wound-induced assembly and closure of an actomyosin purse string in *Xenopus* oocytes. *Curr. Biol.* 9: 579–587.

Benink, H.A., C.A. Mandato, and W.M. Bement. 2000. Analysis of cortical flow models in vivo. *Mol. Biol. Cell.* 11:2553–2563.

Bi, E., P. Maddox, D.J. Lew, E.D. Salmon, J.N. McMillan, E. Yeh, and J.R. Pringle. 1998. Involvement of an actomyosin contractile ring in *Saccharomyces cerevisiae* cytokinesis. *J. Cell Biol.* 142:1301–1312.

Bray, D., and J.G. White. 1988. Cortical flow in animal cells. *Science*. 239:883–888.

Canman, J.C., and W.M. Bement. 1997. Microtubules suppress actomyosin-based cortical flow in *Xenopus* oocytes. *J. Cell Sci*. 110:1907–1917.

Cao, L.G., and Y.L. Wang. 1990. Mechanism of the formation of contractile ring in dividing cultured animal cells. I. Recruitment of preexisting actin filaments into the cleavage furrow. *J. Cell Biol.* 110:1089–1095.

DeBiasio, R.L., G.M. LaRocca, P.L. Post, and D.L. Taylor. 1996. Myosin II transport, organization, and phosphorylation: evidence for cortical flow/solation-contraction coupling during cytokinesis and cell locomotion. *Mol. Biol. Cell.* 7:1259–1282.

Fenteany, G., P.A. Janmey, and T.P. Stossel. 2000. Signaling pathways and cell mechanics involved in wound closure by epithelial cell sheets. *Curr. Biol.* 10: 831–838.

Fishkind, D.J., and Y.L. Wang. 1993. Orientation and three-dimensional organization of actin filaments in dividing cultured cells. *J. Cell Biol.* 123:837–848.

Gunsalus, K.C., S. Bonaccorsi, E. Williams, F. Verni, M. Gatti, and M.L. Goldberg. 1995. Mutations in twinstar, a *Drosophila* gene encoding a cofilin/ADF homologue, result in defects in centrosome migration and cytokinesis. *J. Cell Biol.* 131:1243–1259.

Hird, S.N., and J.G. White. 1993. Cortical and cytoplasmic flow polarity in early embryonic cells of *Caenorhabditis elegans*. *J. Cell Biol.* 121:1343–1355.

Jacinto, A., W. Wood, T. Balayo, M. Turmaine, A. Martinez-Arias, and P. Martin. 2000. Dynamic actin-based epithelial adhesion and cell matching during *Drosophila* dorsal closure. *Curr. Biol.* 10:1420–1426.

Jay, P.Y., P.A. Pham, S.A. Wong, and E.L. Elson. 1995. A mechanical function of myosin II in cell motility. *J. Cell Sci.* 108:387–393.

Kiehart, D.P., C.G. Galbraith, K.A. Edwards, W.L. Rickoll, and R.A. Montague. 2000. Multiple forces contribute to cell sheet morphogenesis for dorsal closure in *Drosophila*. *J. Cell Biol.* 149:471–490.

Kolega, J. 1998. Cytoplasmic dynamics of myosin IIA and IIB: spatial 'sorting' of isoforms in locomoting cells. *J. Cell Sci.* 111:2085–2095.

Lippincott, J., and R. Li. 1998. Sequential assembly of myosin II, an IQGAP-like protein, and filamentous actin to a ring structure involved in budding yeast cytokinesis. *J. Cell Biol.* 140:355–366.

Ma, L., L.C. Cantley, P.A. Janmey, and M.W. Kirschner. 1998. Corequirement of specific phosphoinositides and small GTP-binding protein Cdc42 in inducing actin assembly in *Xenopus* egg extracts. *J. Cell Biol.* 140:1125–1136.

Mandato, C.A., H.A. Benink, and W.M. Bement. 2000. Microtubule-actomyosin interactions in cortical flow and cytokinesis. *Cell Motil. Cytoskeleton*. 45:87–92.

Matsumura, F., S. Ono, Y. Yamakita, G. Totsukawa, and S. Yamashiro. 1998. Specific localization of serine 19 phosphorylated myosin II during cell locomotion and mitosis of cultured cells. *J. Cell Biol.* 140:119–129.

McNeil, P.L., and M. Terasaki. 2001. Coping with the inevitable: how cells repair a torn surface membrane. *Nat. Cell Biol.* 3:E124–E129.

Meeusen, R.L., and W.Z. Cande. 1979. N-ethylmaleimide-modified heavy meromyosin. A probe for actomyosin interactions. *J. Cell Biol.* 82:57–65.

Merriam, R.W., and K. Christensen. 1983. A contractile ring-like mechanism in wound healing and soluble factors affecting structural stability in the cortex of *Xenopus* eggs and oocytes. *J. Embryol. Exp. Morphol.* 75:11–20.

Moores, S.L., J.H. Sabry, and J.A. Spudich. 1996. Myosin dynamics in live *Dictyostelium* cells. *Proc. Natl. Acad. Sci. USA*. 93:443–446.

Motegi, F., K. Nakano, and I. Mabuchi. 2000. Molecular mechanism of myosin-II assembly at the division site in *Schizosaccharomyces pombe*. *J. Cell Sci.* 113: 1813–1825.

Naqvi, N.I., K. Eng, K.L. Gould, and M.K. Balasubramanian. 1999. Evidence for F-actin-dependent and -independent mechanisms involved in assembly and stability of the medial actomyosin ring in fission yeast. *EMBO J.* 18:854–862.

Noguchi, T., and I. Mabuchi. 2001. Reorganization of actin cytoskeleton at the growing end of the cleavage furrow of *Xenopus* egg during cytokinesis. *J. Cell Sci.* 114:401–412.

Poperechnaya, A., O. Varlamova, P.J. Lin, J.T. Stull, and A.R. Bresnick. 2000. Localization and activity of myosin light chain kinase isoforms during the cell cycle. *J. Cell Biol.* 151:697–708.

Raich, W.B., C. Agbunag, and J. Hardin. 1999. Rapid epithelial-sheet sealing in

the *Caenorhabditis elegans* embryo requires cadherin-dependent filopodial priming. *Curr. Biol*. 9:1139–1146.

Rappaport, R. 1996. Cytokinesis in Animal Cells. University Press, Cambridge, UK. 340 pp.

Rozelle, A.L., L.M. Machesky, M. Yamamoto, M. Driessens, R. Insall, M.G. Roth, K. Luby-Phelps, G. Marriott, A. Hall, and H.L. Yin. 2000. Phosphatidylinositol 4,5-bisphosphate induces actin-based movement of raft-enriched vesicles through WASP-Arp2/3. *Curr. Biol*. 10:311–320.

Taunton, J., B.A. Rowning, M.L. Coughlin, M. Wu, R.T. Moon, T.J. Mitchison, and C.A. Larabell. 2000. Actin-dependent propulsion of endosomes and lysosomes by recruitment of N-WASP. *J. Cell Biol*. 148:519–530.

Taylor, D.L., and M. Fechheimer. 1982. Cytoplasmic structure and contractility: the solation-contraction coupling hypothesis. *Philos. Trans. R. Soc. Lond. B. Biol. Sci*. 299:185–197.

Terasaki, M. 1996. Actin filament translocations in sea urchin eggs. *Cell Motil. Cytoskeleton*. 34:48–56.

Verkhovsky, A.B., T.M. Svitkina, and G.G. Borisy. 1999. Self-polarization and directional motility of cytoplasm. *Curr. Biol*. 9:11–20.

Welch, M.D. 1999. The world according to Arp: regulation of actin nucleation by the Arp2/3 complex. *Trends Cell Biol*. 9:423–427.

Welch M.D., A.H. DePace, S. Verma, A. Iwamatsu, and T.J. Mitchison. 1997. The human Arp2/3 complex is composed of evolutionarily conserved subunits and is localized to cellular regions of dynamic actin filament assembly. *J. Cell Biol*. 138:375–384.

White, J.G., and G.G. Borisy. 1983. On the mechanisms of cytokinesis in animal cells. *J. Theor. Biol*. 101:289–316.

Woolley, K., and P. Martin. 2000. Conserved mechanisms of repair: from damaged single cells to wounds in multicellular tissues. *Bioessays*. 22: 911–919.

Yumura, S., and T.Q. Uyeda. 1997. Transport of myosin II to the equatorial region without its own motor activity in mitotic *Dictyostelium* cells. *Mol. Biol. Cell*. 8:2089–2099.

Zang, J.H., and J.A. Spudich. 1998. Myosin II localization during cytokinesis occurs by a mechanism that does not require its motor domain. *Proc. Natl. Acad. Sci. USA*. 95:13652–13657.